Anomalous surface lattice dynamics in the low-temperature phase of $Ba(Fe_{1-x}Co_x)_2As_2$

Jing Teng, Chen Chen, Yimin Xiong, Jiandi Zhang, Rongying Jin, and E. W. Plummer[1]

Department of Physics and Astronomy, Louisiana State University, Baton Rouge, LA 70803-4001

Contributed by E. W. Plummer, December 5, 2012 (sent for review September 7, 2012)

In complex materials, how correlation between charge, spin, and lattice affects the emergent phenomena remains unclear. The newly discovered iron-based high-temperature superconductors and related compounds present to the community a prototype family of materials, where interplay between charge, spin, and lattice degrees of freedom can be explored. With the occurrence of structural, magnetic, and superconducting transitions in the bulk of these materials, creating a surface will change the delicate balance between these phases, resulting in new behavior. A surface lattice dynamics study on (001) $Ba(Fe_{1-x}Co_x)_2As_2$, through electron energy loss spectroscopy measurements, reveals unusual temperature dependence of both the phonon frequency and line width in the low-temperature orthorhombic phase. The rate of change of phonon frequency with temperature is gigantic, two orders of magnitude larger than in the bulk. This behavior cannot be explained using conventional models of anharmonicity or electron–phonon coupling; instead, it requires that a large surface-spin-charge-lattice coupling be included. Furthermore, the higher surface-phase-transition temperature driven by surface stabilization of the low-temperature orthorhombic phase seems to turn the first-order transition (bulk) into the second-order type, equivalent to what is observed in the bulk by applying a uniaxial pressure. Such equivalence indicates that the surface mirrors the bulk under extreme conditions.

spin-lattice coupling | structure transition | magnetic ordering | surface versus bulk

The recent discovery of high-temperature superconductivity in layered iron-based compounds (1) has created enormous activity in the scientific community. One of the most intriguing aspects of these new compounds is the intimate coupling between spin and lattice, offering a wonderful platform to study and manipulate their relationship. The parent compounds (no disorder induced by doping) of the 122 family [Alkaline earth (A) Fe_2As_2] exhibit a coupled magnetic and structural transition from the low-temperature (LT) antiferromagnetic orthorhombic phase to a high-temperature (HT) paramagnetic tetragonal phase (2–4), which has the signature of being first order in the bulk. Fig. 1*A* shows the phase diagram for the compound of interest in this paper, $Ba(Fe_{1-x}Co_x)_2As_2$ (3), where doping the parent compound (Co for Fe) lowers the transition temperatures and at $x \sim 2.2\%$, there seems to be a tricritical point beyond which the magnetic transition becomes second order (2, 4). The strong spin–lattice coupling in these systems (4–7), along with the presence of a tricritical point, creates an environment where either strongly first-order or nearly second-order phase transitions may be observed. Creating a surface by cleaving these layered materials is a controlled way to tip the balance between competing phases, thus providing a unique opportunity to study the subtle aspects of the interactions between lattice and spin through charge. Important for this study is the fact that broken symmetry at the surface creates a significant enhancement in the spin–orbit coupling (8, 9).

Although the nature of the coupled transitions in $BaFe_2As_2$ (Ba122) is still in debate, measurements on the sister compounds $CaFe_2As_2$ (Ca122) and $SrFe_2As_2$ show that the structural and magnetic transitions are discontinuous and hysteretic (i.e., a first-order transition) (2, 4–6). One distinct signature of this coupled transition in the bulk, relevant to this study, is the change in energy and width of the phonon modes as a function of temperature (magnetoelastic coupling) (10–14). Fig. 1*A Inset* shows the energy as a function of temperature for the A_{1g} mode (out-of-plane As vibration) for Ba122 (12), displaying a 0.7% jump to higher energy at the transition into the HT phase, always softer in the LT phase. This trend is in contrast to the modes in Ca122, where the transitions occur at a higher temperature and seem to be more intimately coupled. According to Raman spectroscopy measurements, the B_{1g} mode (out-of-plane vibration of Fe atoms) in Ca122 shows a 1.9% jump at the transition but to lower energy in the HT phase (14). The phonon energy displays a large linear decrease as temperature increases in the LT phase, with a much smaller change in the HT phase. In many aspects, the result presented here is more consistent with the vibrational properties of Ca122 than Ba122. The surface transition temperature is higher than in the bulk mirroring that is seen in the bulk of Ba122 with the application of a uniaxial pressure (15). The temperature dependence of the energy of the surface A_{1g} mode in the LT phase is gigantic, two orders of magnitude larger than in the bulk, a consequence of an enhanced surface spin–lattice coupling.

The close coupling between geometric and magnetic structure in these materials has been the subject of many theoretical papers, of which several are directly relevant to this study. Yin et al. (16) first noted the possibility of strong spin–phonon coupling and found that the magnetism is closely tied to the lattice deformation. Aktürt and Ciraci (17) predicted that phonon modes (associated with the motion of Fe-As) in the HT tetragonal phase of Ba122 will soften in the LT antiferromagnetic orthorhombic phase. This softening is not associated with the traditional mode softening driving structural transition. Yildirim (18) calculated the influence of Fe magnetic moment on the Fe-As and As-As bonding, which changes dramatically as a function of magnetic moment, and pointed out that, through the spin–charge–lattice coupling, spin may play a much more significant role than generally assumed. Mazin and Johannes (19) describe a model with dynamic twin and antiphase spin domain walls that seems to explain many experimental observations, including the temperature separation of the structural and magnetic transitions. Our recent scanning tunneling microscopy (STM) measurements show that the surface can stabilize these dynamic fluctuations at a structural antiphase boundary (20).

Cleaving a single crystal to create a surface breaks the translational symmetry and thus, disturbs the delicate balance between structure and magnetism, which may result in completely new emergent behavior. A hypothetical surface phase diagram for the Co doped Ba122 system, based on the electron energy

Author contributions: J.T., C.C., J.Z., R.J., and E.W.P. designed research; J.T. and C.C. performed research; Y.X. and R.J. contributed new reagents/analytic tools; J.T., C.C., J.Z., R.J., and E.W.P. analyzed data; and J.T., C.C., J.Z., R.J., and E.W.P. wrote the paper.

The authors declare no conflict of interest.

Freely available online through the PNAS open access option.

[1]To whom correspondence should be addressed. E-mail: wplummer@phys.lsu.edu.

This article contains supporting information online at www.pnas.org/lookup/suppl/doi:10.1073/pnas.1220170110/-/DCSupplemental.

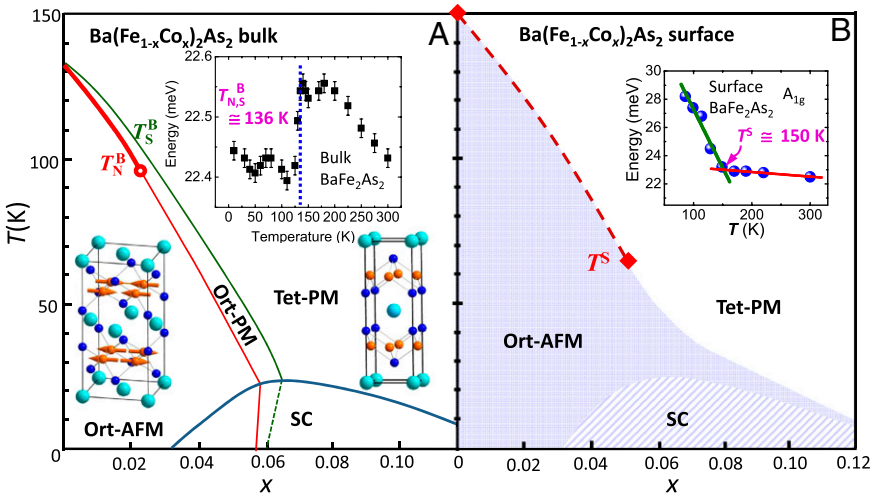

Fig. 1. (*A*) The *T*–*x* phase diagram for bulk $Ba(Fe_{1-x}Co_x)_2As_2$ (3). The thick line denotes a first-order transition, and the thinner lines represent second-order transitions. The open circle denotes the approximate position of a tricritical point (3). (*Insets*) Orthorhombic structure of $BaFe_2As_2$ with in-plane Fe spin marked by arrows (*Left Inset*); tetragonal structure of $BaFe_2As_2$ (*Right Inset*). Raman measurements of the temperature dependence of the peak position of the A_{1g} mode in bulk $BaFe_2As_2$ (12) (*Upper Inset*). (*B*) Proposed *T*–*x* phase diagram for the surface of $Ba(Fe_{1-x}Co_x)_2As_2$ based on the results presented here. (*Inset*) The temperature-dependent phonon shift of A_{1g} surface mode of $BaFe_2As_2$. The transition point is indicated as T^S at 150 K.

loss spectroscopy (EELS) data presented here combined with STM (21), is displayed in Fig. 1*B*. STM studies have shown that the surface stabilizes and enhances the orthorhombic structure throughout the whole range of doping relevant to superconductivity, while maintaining a superconducting gap characteristic of the bulk (21). We report the temperature dependence of two phonon modes for two compositions of $Ba(Fe_{1-x}Co_x)_2As_2$ with $x = 0$ and $x = 0.05$. As summarized in Fig. 1*B*, the observed surface transition temperature is appreciably higher than in the bulk, and the temperature dependence of the vibrational modes in the LT phase is dramatically different from in the bulk. An example is shown in Fig. 1*B Inset*, where the energy of the A_{1g} mode for the compound with $x = 0$ is displayed as a function of temperature, and should be compared with Fig. 1*A Inset* for the bulk mode. The surface surely has tipped the balance between the competing phases.

The technique used in this study is EELS, which is a highly surface-sensitive spectroscopic technique used to probe the dispersion of surface phonons (22). Electrons generated at a cathode are monochromatized and focused onto a sample at energy E_0. The backscattered electrons are both energy- and momentum-resolved. In this experiment, measurements are done in the specularly reflected direction, which means the momentum of the phonon is zero (i.e., the Brillouin zone center). In general, specular scattering probes only the surface infrared active modes. The details of materials preparation and characterization are described in *SI Text*.

Fig. 2*A* displays an EELS spectrum from $Ba(Fe_{0.95}Co_{0.05})_2As_2$ single crystals taken at an incident electron energy $E_0 = 20$ eV and a temperature of 46 K. Three phonon peaks are identified as $\hbar\omega_1$, $\hbar\omega_2$, and $\hbar\omega_3$ with energies 33.5, 26.5, and 14.0 meV, respectively. Based on the previous studies for the bulk (10–14, 17), we can identify these modes (Fig. 2*A Inset*): $\hbar\omega_1$ and $\hbar\omega_2$ are modes associated with Fe and As vibrations, corresponding to the bulk A_{2u} (out-of-plane Fe/As vibration) and the A_{1g} (out-of-plane As vibration), and $\hbar\omega_3$ seems to be related to the E_u mode involving the in-plane stretching vibration of Ba atoms. Both the A_{1g} and E_u modes are Raman active in the bulk but infrared active at the surface. The presence of the surface breaks the inversion symmetry present for the bulk A_{1g} mode. The background is a combination of the instrumental line shape and the Drude spectral weight, which is a measure of the electronic density of states near the Fermi energy (electron/hole excitation spectra). The dashed line is the Drude spectral weight background (*SI Text*). Fig. 2*B* displays the T dependence of the loss spectra for $Ba(Fe_{0.95}Co_{0.05})_2As_2$ after removal of the background. All of the modes soften and broaden as temperature increases.

The data shown in Fig. 2*B* are fit to determine the energy and line width for the intense A_{1g} and A_{2u} modes (*SI Text*), with the results displayed in Fig. 3. Fig. 3 *A* and *C* is for the energy, and Fig. 3 *B* and *D* is for the line width. A simple linear fit (dashed line) to the data in the two temperature regions gives a surface transition temperature of $T^S \sim 65$ K, higher than both the bulk structural transition for $Ba(Fe_{0.95}Co_{0.05})_2As_2$ at 60 K and the magnetic transition at 45 K, as determined from the resistivity data shown in Fig. 3*E*.

Fig. 4 shows the T dependence of the energy and line width of the $\hbar\omega_1$ and $\hbar\omega_2$ phonon modes for the parent compound $BaFe_2As_2$. Notice that the energy of each mode in the HT tetragonal paramagnetic phase is independent on doping level. Fig. 4*A*, a repeat of Fig. 1*B Inset*, is included to enable a detailed

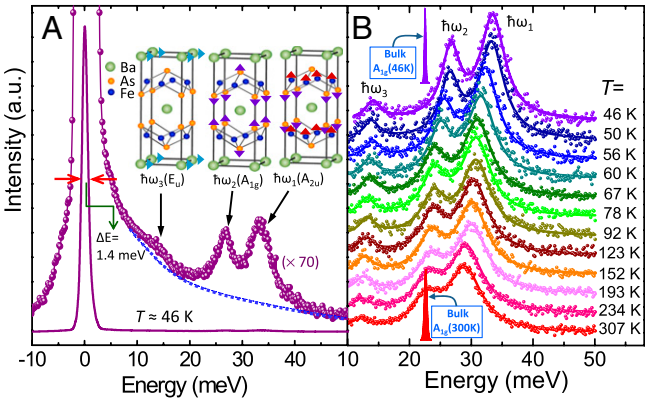

Fig. 2. (*A*) EELS phonon spectra for the surface of $Ba(Fe_{0.95}Co_{0.05})_2As_2$ at 46 K. The blue dotted line is the background caused by the Drude spectral weight. (*Insets*) Schematic representation of the three vibration modes. (*B*) T-dependent spectra with background subtracted. The solid vertical peaks show the energy and width of the bulk A_{1g} mode at 46 and 300 K (12).

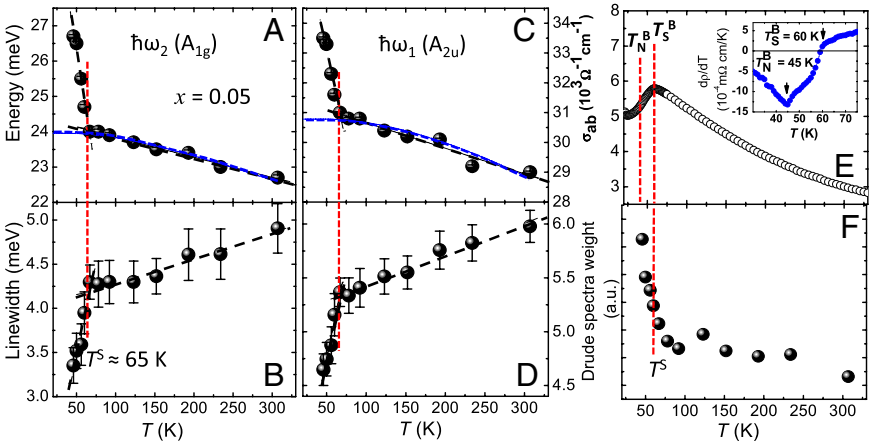

Fig. 3. Data for $Ba(Fe_{0.95}Co_{0.05})_2As_2$. T dependence of the phonon energy and line width of the surface phonon modes $\hbar\omega_2$ (*A* and *B*) and $\hbar\omega_1$ (*C* and *D*). The vertical (red) lines mark the transition at 65 K. The blue line is the fit of the HT data to an anharmonic potential; the line is dashed in the LT phase. The error bars on the energy data are smaller than the width of the data points. (*E*) In-plane conductivity. *Inset* is the derivative of the in-plane resistivity. (*F*) T dependence of Drude weight.

comparison with the bulk A_{1g} mode and a fit using an anharmonic potential. Clearly, the transition temperature $T^S \sim 150$ K for both modes is considerably higher than the coupled bulk structural/magnetic transition at 136 K (Fig. 4*D Inset*). All of modes, for $x = 0$ and $x = 0.05$, exhibit strong T dependence in the LT phase but very gradual (normal) changes in the HT phase. $dE(A_{1g})/dT$ is ~300 times larger at the surface than in the bulk (Fig. 4*A*) in the LT phase. The difference between the bulk and surface for $x = 0.05$ is probably even larger, because the temperature dependence in the bulk is very small (23). Surprisingly, we do not see a discontinuous change in energy at the transition temperature as seen in the bulk (Fig. 1*A Inset*), but with the enhanced line width of ~9.5 meV ($x = 0$) at the transition temperature, the jump would have to be ≥5% to be resolved. The jump observed in the bulk of Ba122 (Fig. 1*A Inset*) is only 0.7% (12). The equivalent number for the jump in Ca122 is 1.9% (14).

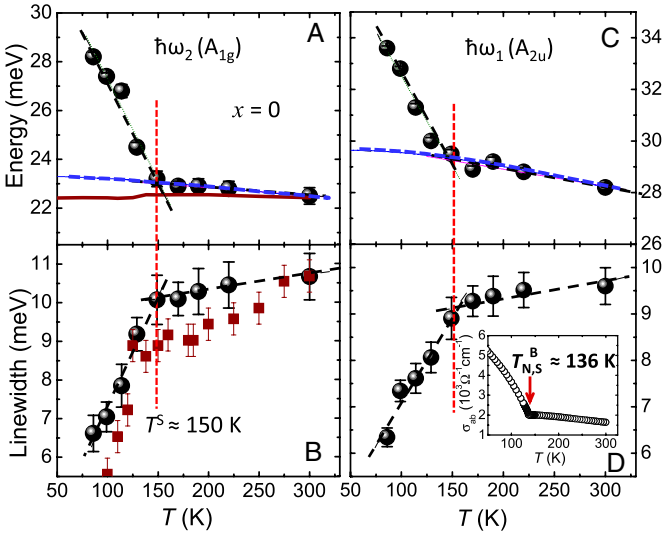

Fig. 4. T dependence of the phonon energy and line width of the surface phonon modes $\hbar\omega_2$ (*A* and *B*) and $\hbar\omega_1$ (*C* and *D*) on $BaFe_2As_2$. The vertical (red) lines mark the transition at 65 K. The blue lines in *A* and *C* are the fit of the HT data to an anharmonic potential; the line is dashed in the LT phase. The solid red line in *A* and the solid red squares with the error bars in *B* are the temperature dependence of frequency and line width of the bulk A_{1g} mode (11). The line width has been normalized (in the text). (*D Inset*) In-plane conductivity of $BaFe_2As_2$ with transition marked with the red arrow.

Although the behavior in the HT phase is similar for both surface and bulk, there is a dramatic difference between the surface and the bulk in the LT phase. As clearly shown in Figs. 3 and 4, there is gigantic softening accompanied by a sharp increase in the line width for the surface phonon modes as temperature increases in the orthorhombic LT phase. Experiment and theory both show that the phonon modes in the bulk for Ba122 (associated with Fe-As vibrations) soften in the orthorhombic phase compared with the tetragonal phase (12, 17) but obviously, not at the surface. As stated previously, the modes for the surface of Ba122 look more like the bulk modes of Ca122 than Ba122. For comparison, we also plot in Fig. 4*A* the data for the A_{1g} mode in the bulk (12) (red solid line), originally displayed in Fig. 1*A Inset*. Both the surface and bulk modes are similar in the HT phase but very different in the LT phase. To illustrate the difference between the surface and bulk in the LT phase, one can compare the T variation of energy (E) and line width (Γ) of the A_{1g} mode in the parent compound: $\frac{dE(A_{1g})}{dT}$ is −83 μeV/K and $\frac{d\,\Gamma(A_{1g})}{dT}$ is +58 μeV/K for the surface. The equivalent numbers for the bulk A_{1g} mode are only −0.27 and +13 μeV/K, respectively.

Before discussing the data shown in Figs. 3 and 4, we would like to point out that the observed behavior cannot be caused by mixing of a surface Brillouin zone center phonon mode with the bulk dispersion of this mode in the direction perpendicular to the surface. Fig. 2*B* shows the energy and width of the bulk A_{1g} mode at 46 and 300 K for the undoped sample (12) compared with the experimental data for $x = 0.05$. Bulk Raman data show very little shift in energy with doping (23). It is clear that the surface A_{1g} mode at LT is appreciably higher in energy than the bulk mode at the bulk Brillouin center. Although there is no bulk phonon dispersion measurement for this compound, it is not expected that such an optical mode would have appreciable dispersion in the direction normal to the plane of a layered material. Data for Sr_2RuO_4 (24) and theoretical calculations for a cuprate (25) and an Fe-based superconductor (26) indicate almost no dispersion perpendicular to the plane. In addition, dispersion of the Ag mode in Sr_2RuO_4 is to lower energy, which would not couple to the higher-energy surface mode. Thus, we believe that the observed behavior reflects the properties of the surface.

Table 1 presents the characteristic values for the phonon modes at the surface and in the bulk (where data are available). In the LT phase, $\frac{dE}{dT}(LT)$ increases by ~300 times for the A_{1g} mode at the surface compared with the bulk ($x = 0$). The slope of the A_{1g}

Table 1. Data for the energies, widths, and temperature-dependent changes in the surface and corresponding bulk phonon modes A_{1g} and A_{2u} (12, 14)

	$dE/dT(LT)$ (μeV/K)	$d\Gamma/dT(LT)$ (μeV/K)	$dE/dT(HT)$ (μeV/K)	$d\Gamma/dT(HT)$ (μeV/K)	E (300 K) (meV)	Γ(300 K) (meV)	X_α	$\hbar\omega_0$ (meV)
Surface								
$A_{1g}(\hbar\omega_2)$ ($x = 0$)	−83.0 ± 9.5	58.2 ± 4.7	−3.2 ± 0.8	4.2 ± 0.6	22.5 ± 2.3	10.6 ± 0.8	0.021 ± 0.003	24.3 ± 0.3
$A_{1g}(\hbar\omega_2)$ (x = 5%)	−138.3 ± 11.7	44.6 ± 6.3	−5.6 ± 0.3	2.6 ± 0.3	22.7 ± 1.4	4.9 ± 0.6	0.030 ± 0.002	25.5 ± 0.1
Bulk								
A_{1g} ($x = 0$)	−0.27	13	−1.1	1.1	22.4	0.94	0.004	22.6
Surface								
$A_{2u}(\hbar\omega_1)$ ($x = 0$)	−69.6 ± 8.4	37.2 ± 4.4	−7.7 ± 1.8	3.9 ± 1.5	28.2 ± 2.3	9.6 ± 0.8	0.035 ± 0.005	31.9 ± 0.5
$A_{2u}(\hbar\omega_1)$ (x = 5%)	−128.5 ± 11.4	35.5 ± 3.9	−8.6 ± 0.8	2.8 ± 0.2	29.0 ± 1.4	6.0 ± 0.5	0.042 ± 0.003	33.6 ± 0.3
Bulk								
Ca B_{1g} (x = 0; 532 nm)	−1.99	5.60	2.01	1.38	25.30	1.24	0.012 ± 0.002	26.3 ± 0.1

mode line width, $\frac{d\Gamma}{dT}(LT)$, is approximately five times larger at the surface than in the bulk. The large value of $\frac{d\Gamma}{dT}(LT)$ at the surface is independent of doping. However, there is significant doping dependence on $\frac{dE}{dT}(LT)$: approximately two times increase for both modes in the doped sample ($x = 0.05$) compared with the undoped compound ($x = 0$)

The corresponding characteristic values [$\frac{dE}{dT}(HT)$, $\frac{d\Gamma}{dT}(HT)$, E (300 K), and Γ(300 K)] for the HT phase are presented in Table 1 as well. At 300 K, the energies of the surface modes are the same for the doped and undoped sample and the same as in the bulk for A_{1g} where data exist. For the undoped samples, there is a three- to fourfold increase in both $\frac{dE}{dT}(HT)$ and $\frac{d\Gamma}{dT}(HT)$ for the A_{1g} mode at the surface compared with the bulk. There is almost no dependence of these quantities on doping level for either mode. The only measurable dependence on doping in the HT phase is the width at 300 K. The modes in the undoped sample have approximately two times the width as in the doped sample, which is counter to the idea that Co dopant will create disorder but consistent with the differences in $\frac{d\Gamma}{dT}(HT)$.

Historically, the change in energy and line width of a surface vibration mode with temperature has been modeled with a simple anharmonic potential, such as a Moorse potential (27, 28). Although it is easy to explain the T dependence of the modes in the HT phase, the mode energy and width in the LT phase cannot be fit using such a simple approach. With an anharmonic potential, the energy between adjacent states is $\Delta E = E_n - E_{n-1} = (1 - 2X_\alpha n)\hbar\omega_0$, where X_α is a dimensionless measure of the anharmonicity (29). When fitting the temperature dependence of the data, there are two parameters, X_α and $\hbar\omega_0$. All of the results from the fitting are included in Table 1. For an ordinary metal surface, such as Cu(110), X_α is ∼0.032 compared with 0.015 in the bulk (27). The fitting for the HT phase A_{1g} surface mode is shown in both Fig. 4*A* for $x = 0$ and Fig. 3*A* for $x = 0.05$. For the parent compound, $X_\alpha = 0.021$ and $\hbar\omega_0 = 23.3$ meV, whereas $X_\alpha = 0.030$ and $\hbar\omega_0 = 24.0$ meV for $x = 0.05$. A fit for the HT bulk A_{1g} mode (Fig. 4*A*) gives $\hbar\omega_0 = 22.6$ meV with $X_\alpha = 0.004$. These fits give a quite reasonable explanation for the T dependence of the HT modes. The surface has an enhanced anharmonicity as expected (27), but the zero temperature mode energy $\hbar\omega_0$ is almost the same for the surface and bulk, and there is no variation with doping. However, the unusual phonon behavior in the LT phase cannot be explained with such a simple model.

Fig. 3*E* is a plot of the T dependence of in-plane electrical conductivity measured from the single crystal used in this experiment (5% Co doping). Note that, with increasing temperature, conductivity increases until it reaches a maximum at ∼ 60 K and then decreases. Fig. 3*E Inset* shows $\frac{d\rho_{ab}}{dT}$ vs. T and indicates the procedure to identify the magnetic transition temperature T_N ($\frac{d\rho_{ab}}{dT}$ maximum) and the structural transition T_S ($\frac{d\rho_{ab}}{dT} = 0$). Fig. 3*F* is the measured Drude weight (*SI Text*) obtained from the background shown in Fig. 2*A*. It is quite apparent that there is almost no correspondence between the surface Drude weight (surface metallicity) and the bulk in-plane conductivity. However, if the Drude weight for the doped compound is compared with the in-plane conductivity for the parent compound (Fig. 4*D Inset*), the two are very similar. They fall rapidly as the temperature increases in the LT phase but are much less temperature-dependent in the HT phase. With the lack of a nonmonotonic T dependence of the Drude spectral weight (Fig. 3*F*), we conclude that the surface magnetic and structural transitions occur at approximately the same temperature for $x = 0.05$ compound, which is what was implied in the surface phase diagram in Fig. 1*B*. The continuous nature of the temperature dependence of both energy and line width for $x = 0$ and $x = 0.05$ suggests the absence of a tricritical point at surface.

The dramatic phonon broadening and the sharp phonon softening as $T \to T^S$ unambiguously indicate that the observed surface phonon modes have strong interactions with both charge and spin degrees of freedom. As shown in Fig. 3*F*, the Drude weight decreases rapidly with increasing temperature in the LT phase, indicating the decrease of spectral weight in low-energy electron–hole pair excitation. If the ordinary electron–phonon coupling (EPC; in the nonmagnetic case) is the only channel for phonon decay through electron–hole pair excitations, thus causing phonon broadening, one would not anticipate such a substantial increase of phonon line width as $T \to T^S$. In a simple approximation, the probability of phonon decay through EPC is proportional to magnitude of the low-energy electron–hole pair excitations. In Fe-based superconductors, recent theoretical studies indicate that the EPC is weak (30), and angle-resolved photoemission spectroscopy (ARPES) data do not show a large renormalization of the bands near the Fermi energy (31). Another channel for phonon decay is associated with a strong spin–phonon interaction, such that the change of spin structure may significantly renormalize the phonon energy and lifetime. Because the two phonon modes discussed here are in the As-Fe layer associated with the magnetic ions, spin–charge–lattice coupling should be included, caused by the modulation of the spin exchange integral by lattice vibrations (32–36). It should be pointed out that one cannot talk about spin–phonon interaction without the involvement of EPC (35, 36) or spin–orbit coupling (37).

Spin–phonon coupling exists throughout the whole temperature range but only induces a coherent shift of phonon energy in the magnetically ordered phase. When $T > T^S$, the coupling goes incoherent, which results in (*i*) large phonon peak broadening (incoherence shortens the phonon lifetime) and (*ii*) anharmonicity-induced broadening that dominates the temperature dependence of phonon modes in the HT paramagnetic phase. In $BaFe_2As_2$, the displacement patterns of both A_{1g} (As antiphase vibration) and A_{2u} (mixed Fe/As vibration) modes

distort the Fe-As-Fe bond angles, which are involved in the J_{1a} and J_{1b} exchange integrals. All of the short-range exchange integrals between Fe ions occur through the As orbitals. Any phonon with the lattice vibration in the Fe/As layer should transmit the magnetic interaction and simultaneously modulate the phonon behavior. In the paramagnetic phase with no spin ordering and only the incoherent spin–phonon interaction, the weak temperature dependence of energy reflects only the contribution of anharmonicity. As soon as the system enters the magnetically ordered phase, marked effects caused by magnetic exchange interactions in phonon behavior are expected. This feature is in accordance with other studies of $Ba(Fe_{1-x}Co_x)_2As_2$ (18) and LaFeAsO (19), which show strong coupling of the phonon spectra with the magnetic moment of Fe sublattices. Our data indicate that such coupling is enhanced at the surface.

Evidently, the surface amplifies the spin–lattice coupling, leading to a stronger phonon anomaly than in the bulk. As mentioned previously, the presence of a surface enhances the orthorhombicity, which promotes both spin ordering and spin–orbit coupling. Therefore, there is a surface-enhanced magnetoelastic interaction in the LT phase, leading to the higher structural/magnetic transition temperature at the surface ($T^S = 65$ K for $x = 0.05$ and 150 K for $x = 0$).

The obvious question is why the surface induces gigantic changes in lattice dynamics for $Ba(Fe_{1-x}Co_x)_2As_2$. The first clue comes from a neutron scattering study of the effect of uniaxial pressure on the coupled structural/magnetic-phase transition in $BaFe_2As_2$ (15). The application of a critical pressure of 0.7 MPa, beyond the pressure needed to detwin the sample, dramatically increases the structural transition temperature (~147 K) accompanied by the onset of long-range magnetic ordering at the same temperature. As shown above, the surface transition temperature for $BaFe_2As_2$ is very close to the temperature observed by the application of a uniaxial pressure. Although it is difficult experimentally to quantify the induced strain along all directions by creating the surface, the observation of surface-enhanced orthorhombicity suggests that the surface behaves similarly to the bulk sample under uniaxial pressure, increasing the structural transition temperature concomitant with long-range magnetic ordering, both with second-order–like characteristics (15). The second clue is the dramatic 10-fold increase in the line width in the HT phase at 300 K for the A_{1g} mode (column 8 in Table 1). This observation is a clear indication that the spin–lattice coupling through incoherent spin fluctuations is an order of magnitude higher at the surface, dramatically decreasing the lifetime of the mode. To illustrate this behavior, Fig. 4*B* shows the line width measured for the A_{1g} mode in the bulk (12) normalized to the surface line width at 300 K (Table 1). If, by the application of a uniaxial pressure in the bulk, the spin–lattice coupling could be increased to what it is at the surface, the bulk would look like the surface. The final observation is that the presence of the enhanced orthorhombicity at the surface stiffens the LT modes appreciably. An extrapolation of the energy of the surface A_{1g} mode to $T = 0$ K for the parent compound gives $\hbar\omega_{1g}(T = 0\ \text{K}) = 36.7$ meV compared with the bulk energy of 22.44 meV. Everything that we observe can be rationalized with increased spin–lattice coupling, coherent in the LT phase. The differences in the doped sample must again reflect a decrease in the spin–lattice coupling at the surface because of Co doping. For example, $\hbar\omega_{1g}(T = 0\ \text{K}) = 33.0$ meV is lower for $x = 0.05$, and its line width at 300 K is only 46% of the linewidth of the parent compound.

In conclusion, EELS results reveal dramatic temperature dependence both in the energy and width of the two dipole-active modes A_{1g} and A_{2u} in the LT phase of both the parent and Co-doped $BaFe_2As_2$. This behavior is in contrast to the behavior of these phonon modes in the HT phase, which is nearly identical to the bulk and can be explained within a simple anharmonic potential model. The surface transition temperature T^S is higher than in the bulk, most likely driven by the strain induced by creating a surface. The surface strain enhances orthorhombicity, raises the transition temperatures, and restores the concomitant magnetic and structural transitions, even for $x = 0.05$ Co doping. These features mirror the bulk properties under uniaxial stress (15). Hence, our surface measurements resolve the question of the origin of the increase in magnetic ordering in the bulk under the application of a uniaxial pressure. It is a consequence of strong spin–lattice coupling in this system.

ACKNOWLEDGMENTS. We thank Wei Ku, Indranil Paul, and David Mandrus for very useful discussions. This research was primarily supported by National Science Foundation Grant DRM 1002622. J.T. received support from the office of the Vice Chancellor for Research at Louisiana State University. J.Z. received support from National Science Foundation Grant DMR 1005562.

1. Kamihara Y, Watanabe T, Hirano M, Hosono H (2008) Iron-based layered superconductor La[$O_{(1-x)}F_{(x)}$]FeAs (x = 0.05-0.12) with T_c = 26 K. *J Am Chem Soc* 130(11): 3296–3297.
2. Kim MG, et al. (2011) Character of the structural and magnetic phase transitions in the parent and electron-doped $BaFe_2As_2$ compounds. *Phys Rev B* 83(13):134522.
3. Nandi S, et al. (2010) Anomalous suppression of the orthorhombic lattice distortion in superconducting $Ba(Fe_{1-x}Co_x)_2As_2$ single crystals. *Phys Rev Lett* 104(5): 057006.
4. Goldman AI, et al. (2008) Lattice and magnetic instabilities in $CaFe_2As_2$: A single-crystal neutron diffraction study. *Phys Rev B* 78(10):100506.
5. Jesche A, et al. (2008) Strong coupling between magnetic and structural order parameters in $SrFe_2As_2$. *Phys Rev B* 78(18):180504.
6. Wilson S, et al. (2009) Neutron diffraction study of the magnetic and structural phase transitions in $BaFe_2As_2$. *Phys Rev B* 79(18):184519.
7. Egami T, et al. (2010) Spin-lattice coupling and superconductivity in Fe pnictides. *Adv Condens Matter Phys* 2010:164916.
8. LaShell S, McDougall BA, Jensen E (1996) Spin splitting of an Au(111) surface state band observed with angle resolved photoelectron spectroscopy. *Phys Rev Lett* 77(16): 3419–3422.
9. Rothenberg E, Chung JW, Kevan SD (1999) Spin-orbit coupling induced surface band splitting in Li/W(110) and Li/Mo(110). *Phys Rev Lett* 82(20):4066–4069.
10. Choi KY, et al. (2010) Self-energy effects and electron-phonon coupling in Fe-As superconductors. *J Phys Condens Matter* 22(11):115802.
11. Akrap A, et al. (2009) Infrared phonon anomaly in $BaFe_2As_2$. *Phys Rev B* 80(18): 180502.
12. Rahlenbeck M, et al. (2009) Phonon anomalies in pure and underdoped $R_{1-x}K_xFe_2As_2$ (R=Ba,Sr) investigated by Raman light scattering. *Phys Rev B* 80(6):064509.
13. Chauvière L, et al. (2009) Doping dependence of the lattice dynamics in $Ba(Fe_{1-x}Co_x)_2As_2$ studied by Raman spectroscopy. *Phys Rev B* 80(9):094504.
14. Choi KY, et al. (2008) Lattice and electronic anomalies of $CaFe_2As_2$ studied by Raman spectroscopy. *Phys Rev B* 78(21):212503.
15. Dhital C, et al. (2012) Effect of uniaxial strain on the structural and magnetic phase transitions in $BaFe_2As_2$. *Phys Rev Lett* 108(8):087001.
16. Yin ZP, et al. (2008) Electron-hole symmetry and magnetic coupling in antiferromagnetic LaFeAsO. *Phys Rev Lett* 101(4):047001.
17. Aktürk E, Ciraci S (2009) First-principles study of the iron pnictide superconductor $BaFe_2As_2$. *Phys Rev B* 79(18):184523.
18. Yildirim T (2009) Strong coupling of the Fe-spin state and the As-As hybridization in iron-pnictide superconductors from first-principle calculations. *Phys Rev Lett* 102(3): 037003.
19. Mazin II, Johannes MD (2009) A key role for unusual spin dynamics in ferropnictides. *Nat Phys* 5(2):141–145.
20. Li G, et al. (2012) Coupled structural and magnetic antiphase domain walls on $BaFe_2As_2$. *Phys Rev B* 86(6):060512.
21. Pan SH, et al. (2011) STM studies of the lattice distortion at the surface of $Ba(Fe_{1-x}Co_x)_2As_2$. *Bulletin of the American Physical Society*. Available at http://meetings.aps.org/Meeting/MAR11/Event/137180.
22. Ibach H (1977) *Electron Spectroscopy for Surface Snalysis* (Springer, Berlin).
23. Chauvière L, et al. (2011) Raman scattering of spin-density-wave order and electron-phonon coupling in $Ba(Fe_{1-x}Co_x)_2As_2$. *Phys Rev B* 84(10):104508.
24. Braden M, Reichardt W, Sidis Y, Mao Z, Maeno Y (2007) Lattice dynamics and electron-phonon coupling in Sr_2RuO_4: Inelastic neutron scattering and shell-model calculations. *Phys Rev B* 76(1):014505.
25. Kress W, Schröder U (1988) Lattice dynamics of the high-T_C superconductor $YBa_2Cu_3O_{7-x}$. *Phys Rev B* 38(4):2906–2909.
26. Singh DJ, Du MH (2008) Density functional study of LaFeAsO$_{(1-x)}$F$_{(x)}$: A low carrier density superconductor near itinerant magnetism. *Phys Rev Lett* 100(23):237003.
27. Baddorf AP, Plummer EW (1990) Surface anharmonicity: Temperature dependence of phonon energies on Cu(110). *J Electron Spectrosc Relat Phenom* 54:541–550.

28. Herzberg G (1989) *Molecular Spectra and Molecular Structure: I. Spectra of Diatomic Molecules* (Krieger, Malabar, FL).
29. Rosenstock H (1974) Multiphonon absorption in alkali halides: Quantum treatment of morse potential. *Phys Rev B* 9(4):1963–1970.
30. Boeri L, Dolgov OV, Golubov AA (2008) Is $LaFeAsO_{1-x}F_x$ an electron-phonon superconductor? *Phys Rev Lett* 101(2):026403.
31. Liu C, et al. (2008) K-doping dependence of the Fermi surface of the iron-arsenic $Ba_{1-x}K_xFe_2As_2$ superconductor using angle-resolved photoemission spectroscopy. *Phys Rev Lett* 101(17):177005.
32. Lockwood DJ, Cottam MG (1988) The spin-phonon interaction in FeF_2 and MnF_2 studied by Raman spectroscopy. *J Appl Phys* 64(10):5876–5878.
33. Saha S, et al. (2008) Temperature-dependent Raman and x-ray studies of the spin-ice pyrochlore $Dy_2Ti_2O_7$ and nonmagnetic pyrochlore $Lu_2Ti_2O_7$. *Phys Rev B* 78(21): 214102.
34. Granado E, et al. (1999) Magnetic ordering effects in the Raman spectra of $La_{1-x}Mn_{1-x}O_3$. *Phys Rev B* 60(17):11879–11882.
35. Yndurain F, Soler JM (2009) Anomalous electron-phonon interaction in doped LaFeAsO: First-principle calculations. *Phys Rev B* 79(13):134506.
36. Boeri L, Calandra M, Mazin II, Dolgov OV, Mauri F (2010) Effects of magnetism and doping on the electron-phonon coupling in $BaFe_2As_2$. *Phys Rev B* 82(2):020506.
37. Marn FP, Suhl H (1989) Spin-orbit coupling modulated by the electron-phonon interaction. *Phys Rev Lett* 63(4):422–444.